AGU PUBLICATIONS

JGR

Journal of Geophysical Research: Space Physics

RESEARCH ARTICLE
10.1002/2016JA022696

Key Points:
- Three types of electron scattering can occur in a whistler chorus element
- Phase-trapping process causes a rapid flux enhancement of electrons
- MeV electron flux can increase in a time scale of minutes

Correspondence to:
S. Saito,
s.saito@nagoya-u.jp

Citation:
Saito, S., Y. Miyoshi, and K. Seki (2016), Rapid increase in relativistic electron flux controlled by nonlinear phase trapping of whistler chorus elements, *J. Geophys. Res. Space Physics*, *121*, 6573–6589, doi:10.1002/2016JA022696.

Received 24 MAR 2016
Accepted 25 JUN 2016
Accepted article online 1 JUL 2016
Published online 23 JUL 2016

Rapid increase in relativistic electron flux controlled by nonlinear phase trapping of whistler chorus elements

Shinji Saito[1], Yoshizumi Miyoshi[2], and Kanako Seki[3]

[1]Graduate School of Science, Nagoya University, Nagoya, Japan, [2]Institute for Space-Earth Environmental Research, Nagoya University, Nagoya, Japan, [3]Department of Earth and Planetary Science, Graduate School of Science, University of Tokyo, Hongo, Japan

Abstract Wave-particle interactions with whistler chorus waves are believed to provide a primary acceleration for electrons in the outer radiation belt. Previous models for flux enhancement of the radiation belt have assumed the stochastic process as a diffusion manner of successive random-phase interactions, but physical mechanisms for the acceleration are not fully incorporated in these models because of the lack of a nonlinear scattering process. Here we report rapid increase in relativistic electron flux by using an innovative computer simulation model that incorporates not only diffusive process but also nonlinear scattering processes. The simulations show that three types of scattering simultaneously occur, which are diffusive, phase trapping, and phase bunching. It is found that the phase trapping is the most efficient mechanism to produce the MeV electrons rapidly in the scattering processes. The electrons are accelerated from 400 keV to over 1 MeV in time scale less than 60 s. On the other hand, as the phase trapping is suppressed by the breaking of relative phase angle between waves and gyrating electrons during the interaction, the increase of electron flux at MeV energy is clearly reduced. Our simulations conclude that the phase-trapping process causes a significant effect for the increase in relativistic electron flux and suggest that a quasi-linear diffusion model is not always valid to fully describe the relativistic electron acceleration.

1. Introduction

The Van Allen radiation belts consist of electrons with energies higher than a few hundreds keV in the Earth's magnetosphere. There are two plausible mechanisms for the flux enhancement of the outer radiation belt in the magnetosphere, which are inward diffusion and local wave acceleration. Trapped electrons encircling the Earth at a time scale around a few hundreds of seconds resonate with magnetohydrodynamic waves, which are ultralow frequency (ULF) waves of a few millihertz in the magnetosphere, and are transported in a radial direction due to a drift-resonant interaction [*Elkington et al.*, 1999]. When the resonant electrons are transported toward the Earth where the magnetic field intensity becomes higher, they are accelerated by conserving the first adiabatic invariant.

The other promising candidate for flux enhancement is a local wave acceleration by cyclotron resonance. Recent observations have shown that the local acceleration can explain a production of relativistic electrons in the heart of the outer radiation belt [*Miyoshi et al.*, 2003, 2007, 2013; *Chen et al.*, 2007; *Reeves et al.*, 2013]. A potential candidate for the cause of the local acceleration is whistler wave [*Summers et al.*, 1998; *Meredith et al.*, 2002; *Miyoshi et al.*, 2003]. Electrons can resonate with the whistlers as the cyclotron resonance condition $\omega - k_{||} v_{||} = n\Omega_e/\gamma$ is satisfied, where ω, $k_{||}$, $v_{||}$, Ω_e, and γ are the wave angular frequency, parallel wave number, parallel electron velocity, electron cyclotron angular frequency, and relativistic Lorentz factor, respectively. Here n is integer with $n > 0$.

A quasi-linear diffusion model has been widely used to describe the local wave acceleration. Simulations under the quasi-linear model [e.g., *Miyoshi et al.*, 2003; *Horne et al.*, 2005; *Thorne et al.*, 2013] suggest that whistler waves can cause rapid flux enhancement as observed in the outer radiation belt at a time scale of about a few hours. Hence, ULF waves may not always be necessary to explain the increase in the relativistic electron flux. In addition, *Horne et al.* [2005] found that in the huge Halloween geomagnetic storms that occurred between 29 October and 4 November 2003, wave-particle interactions with whistler waves were a more likely explanation of the intense electron flux enhancement than ULF waves.

The quasi-linear theory assumes that whistler waves are typically small in amplitude and have multiple random-phase interactions with electrons. However, the whistler waves observed during geomagnetic storms are not only incoherent band of waves, so-called plasmaspheric hiss [*Thorne et al.*, 1973; *Bortnik et al.*, 2008a, 2009], but also coherent, discrete, and intense electromagnetic waves, so-called whistler chorus waves. Recently, fine structure of spectral density in plasmaspheric hiss is also observed, which shows that plasmaspheric hiss could consist of large amounts of coherent whistler waves [*Summers et al.*, 2014]. Whistler chorus waves consist of several discrete elements within a burst emission, each lasting for a few tens to hundreds of milliseconds, and have a typical frequency drift rate of about a few kHz/s [*Santolík et al.*, 2003]. Since the chorus waves are certainly nonlinear waves, which consist of discrete elements and have rising and/or falling tone of frequency, the wave-particle interactions can be a cause of nonlinear scattering of electrons.

The wave-particle interactions cause three types of scattering: diffusive, phase-trapping, and phase-bunching processes [*Albert*, 2002; *Bortnik et al.*, 2008b]. The diffusive scattering can be treated as statistical changes in pitch angle and energy, which is quasi-linear diffusion model. On the other hand, phase trapping and phase bunching are nonlinear processes due to a finite amplitude of whistler wave, which are not described by the diffusive process. The phase trapping efficiently increases pitch angle and energy of a few electrons in a short time scale, while the phase bunching leads to collective behavior of electrons in pitch angle and energy. *Albert* [2002] argues that the diffusive process is too slow, while phase bunching leads to only deceleration. Only phase trapping is expected to accelerate electrons from some 0.1 MeV to about 1 MeV in about 1 min. *Bortnik et al.* [2008b] also identifies three types of scattering using test-particle simulation. The phase bunching leads to collective deceleration of electrons independent of relative phase angle between electron gyration phase and wave phase, and the phase-trapping process leads to rapid energy gain in large wave amplitude.

Motion of phase-trapped electron with relativistic effect has been studied. *Omura et al.* [2007] show that a finite amplitude, coherent, monochromatic whistler wave can accelerate electrons from a few hundreds keV to MeV energy within a second. *Furuya et al.* [2008] develop the phase-trapping theory by including the frequency drift of whistler chorus. While this acceleration process is more efficient than acceleration by the diffusive process, only a few electrons are accelerated [*Omura et al.*, 2007; *Furuya et al.*, 2008] in a coherent, monochromatic whistler wave. In addition, intermittent changes of frequency and direction of wave number vector in a raising tone whistler chorus element [*Santolík et al.*, 2014], which would cause intermittent breaking of phase angle between whistler waves and gyrating electrons (hereafter, we refer the intermittent breaking process as "the phase angle breaking"), suggest to reduce the acceleration efficiency of phase-trapped electrons. Further, the multiple scatterings by whistler chorus elements may be equivalent to the quasi-linear diffusion process because the electron is successively scattered by whistler waves with broadband frequency and uncertain wave phase. Thus, one may consider that electron acceleration by the phase trapping is not essential for the flux enhancement of relativistic electrons, especially over the time scale of a geomagnetic storm. However, this consideration is not trivial. Even if only a few electrons were transported into relativistic energies by the interactions with the chorus element, many interactions during a geomagnetic storm may produce more efficient net flux enhancement than that with only quasi-linear diffusive process.

In this paper, we use the Geospace Environment Modeling System for Integrated Studies-Radiation Belt with Wave-Particle Interaction (GEMSIS-RBW), an innovative test-particle simulation code, to examine the role of nonlinear scattering process for the net flux enhancement of relativistic electrons. Section 2 introduces parameters to set up the physical condition, and section 3 shows the simulation results. Discussions for three types of scattering process and the flux increase controlled by the phase angle breaking are described in section 4. Finally, we make a summary in section 5. In Appendixes A and B, we introduce a basic concept of GEMSIS-RBW model and a theoretical description of an equilibrium phase angle of electron trapped in whistler wave on a magnetic field line.

2. Simulation Parameters

The GEMSIS-RBW is used to demonstrate wave-particle interactions between electrons and whistler chorus elements. The electrons have the initial kinetic energy 400 keV and are located on a dipole magnetic field line at $L = 4$ with random bounce phase. Lower band whistler chorus elements are given at the equator of the dipole field line. An element lasts for $t_{\mathrm{element}} = 1.25$ s with a frequency sweep rate $\mathrm{d}\omega/\mathrm{d}t = 0.32\Omega_{e,\mathrm{eq}}$ rad/s^2 at the equator. Here $\Omega_{e,\mathrm{eq}}$ is the electron cyclotron angular frequency at the equator. The frequency ranges

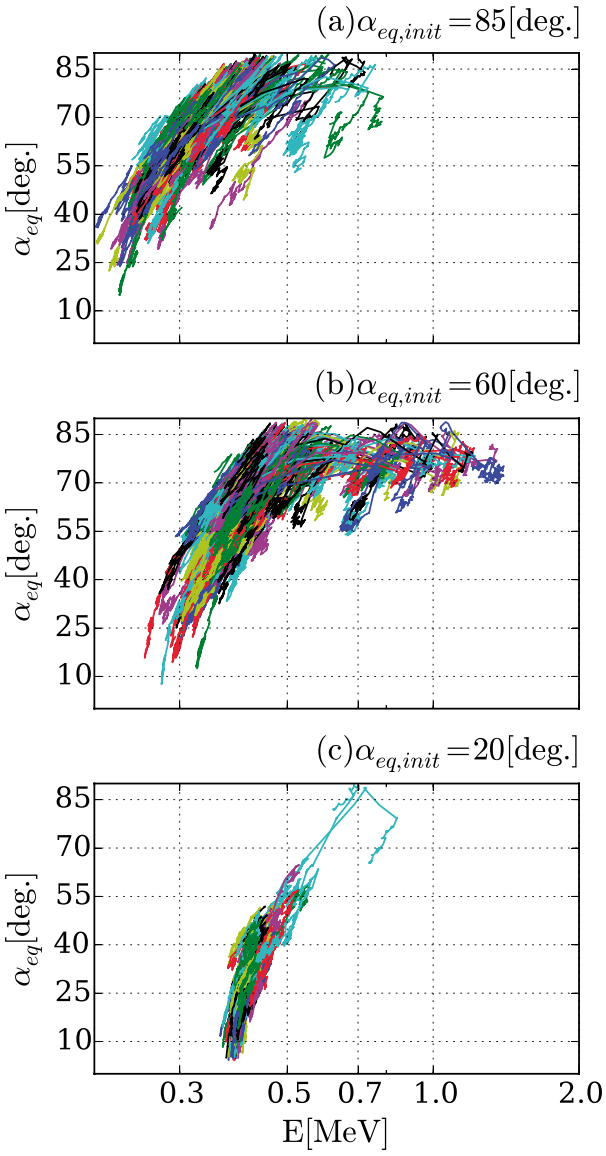

Figure 1. Electron trajectories during 60 s for three simulation runs (f_{PB} = 0 Hz) with the initial kinetic energy 400 keV and with (a) $\alpha_{eq,init}$ = 85°, (b) $\alpha_{eq,init}$ = 60°, and (c) $\alpha_{eq,init}$ = 20°, where the pitch angle is equatorially mapped. Each run has 128 electrons.

from $0.1\Omega_{e,eq}$ to $0.5\Omega_{e,eq}$. We assume that these elements are continuously generated every $t_{element}$ at the equator and propagate parallel/antiparallel to the magnetic field with their group velocity. The amplitude of the wave is assumed to be 120 pT. The lower band chorus waves with amplitude larger than 100 pT is frequently observed especially during disturbed geomagnetic conditions [*Macúšová et al.*, 2015]. Frequency ratio between electron plasma and electron cyclotron angular frequency is $\omega_e/\Omega_{e,eq}$ = 1.7, where the background plasma density is assumed to be constant along the magnetic field. Here we assume relatively low density situation at L = 4 similar to [*Omura et al.*, 2007]. The time step for the adiabatic motion of electron is Δt = 1 ms. The time resolution for electron cyclotron motion associated with the nonadiabatic momentum change in waves is $\Delta t_w \sim 2\pi(\Omega_e N)^{-1}$, where Ω_e is the electron cyclotron angular frequency at the electron position, and we choose N = 60 to fully resolve the cyclotron motion. Explanation for Δt and Δt_w is described in Appendix A.

3. Results

In this section we show simulation results of wave-particle interactions in the case of coherent and incoherent whistler chorus elements. In simulations with the coherent whistler chorus waves, a set of equations ((A6)–(A8)) calculates the phase angle between electron and whistler wave. On the other hand, in simulations with the incoherent waves, equation (A9) is additionally used to consider the relative phase angle breaking which occurs every f_{PB}^{-1} during the interaction. Here the phase angle breaking means the intermittent breaking process of the relative phase angle between whistler waves and electrons. After showing physics of the wave-particle interactions in the coherent/incoherent whistler chorus elements, we show a flux enhancement at relativistic energies accelerated from 400 keV electrons with pitch angle distribution proportional to $\sin\alpha_{eq}$.

3.1. Electron Scattering by Whistler Chorus Elements With f_{PB} = 0 Hz

Figure 1 shows electron trajectories on (E, α_{eq}) plane during 60 s for three simulation runs, where E is the kinetic energy and α_{eq} is the equatorial pitch angle. Three panels show results of three initial equatorial pitch angle $\alpha_{eq,init}$ = (a) 85°, (b) 60°, and (c) 20°. Each simulation has 128 electrons with kinetic energy 400 keV at t = 0. In all runs, the energy of electrons increases (decreases) with increasing (decreasing) pitch angle. The common feature indicates electrons are in cyclotron resonance with a counterpropagating whistler wave.

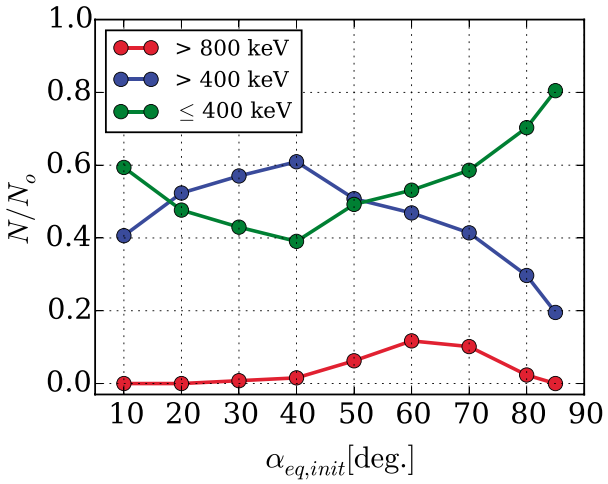

Figure 2. The number of decelerated, accelerated, and strongly accelerated electrons at 60 s as a function of the initial pitch angle. These numbers are normalized to the total number of electrons in each run.

However, trajectories in Figures 1a–1c are different from each other. The nature of scattering depends on the initial pitch angle.

Figure 2 shows the number of decelerated (green line: $E \leq 400$ keV), accelerated (blue line: $E > 400$ keV), and strongly accelerated electrons (red line: $E > 800$ keV) at 60 (s) as a function of $\alpha_{eq,init}$, which are normalized to the total number of electrons in each run. As shown by the red line, 11.7% of electrons with $\alpha_{eq,init} = 60°$ are accelerated to relativistic energies over 800 keV within 60 s. On the other hand, there is a noticeable electron deceleration at large pitch angles as seen in the green line. At $\alpha_{eq,init} = 85°$, over 80% of electrons are decelerated from 400 keV. At smaller pitch angles ($\alpha_{eq,init} < 70°$), however, the green and blue lines show that the number of decelerated and accelerated electrons is nearly equal. This result indicates that the diffusive process is dominant at relatively small pitch angles, while at larger pitch angles, the scattering includes two nonlinear processes. One process strongly accelerates a few electrons around $\alpha_{eq,init} = 60°$, the other process effectively decelerates a lot of electrons at $\alpha_{eq,init} > 70°$.

Figure 3 shows time development of energy of electrons with $\alpha_{eq,init} = 85°$. Figure 3a shows the development of 128 electrons in 60 s. While we can find a few electrons rapidly increase energy, about 80% of total electrons (as seen in Figure 2) decreases their energy. Figure 3b shows temporal evolution of energy of five electrons from 1.0 to 1.2 s. Here these electrons are arbitrarily selected from electrons plotted in Figure 3a. Each electron is scattered to lower energies in a short time scale (10 (ms) or less) at several times. The energy decrease seems to be intermittent, not to be gradual decrease like a diffusion process. The collective deceleration of the electrons is due to the phase-bunching process shown in *Bortnik et al.* [2008b], which is completely nonlinear process.

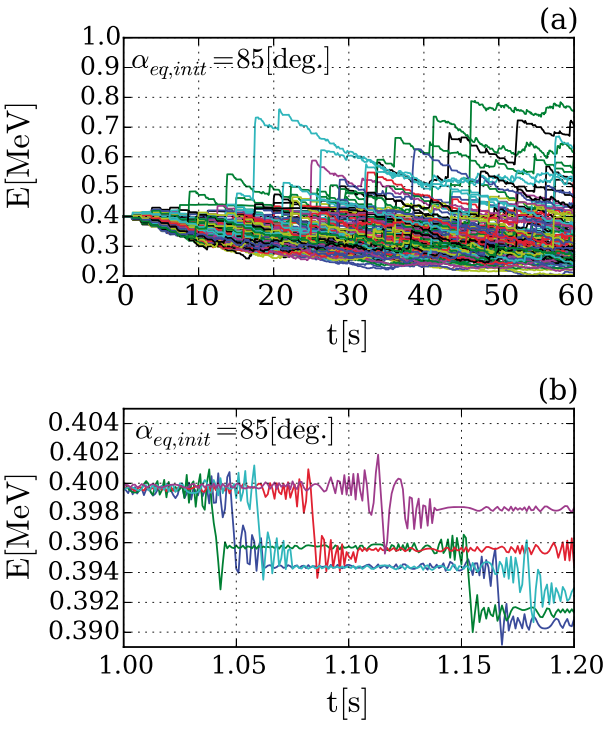

Figure 3. Time development of energy with $\alpha_{eq,init} = 85°$. (a) Energy of 128 electrons for 60 s. (b) Energy of five electrons from 1.0 to 1.2 s.

Figure 4 shows trajectories of a rapidly accelerated electron with $\alpha_{eq,init} = 60°$. Figure 4a shows a trajectory of the electron in (z, E) plane, where z is the distance from the equator along the field line and E is the electron energy. Circles are time stamps as shown by the color scale of time. The electron moves from the Southern Hemisphere ($z < 0$) to the Northern Hemisphere ($z > 0$). The magnetic mirror force reflects the electron at $z \sim 0.9\ R_E$, where R_E is the Earth radii. When the electron goes back to the equator after the mirror reflection, the electron gains the energy 519 keV in 280 ms. The trajectory of Figure 4a is quite similar to that shown in preceding papers [*Omura et al.*, 2007; *Furuya et al.*, 2008] studying elementary motion of the phase-trapped electron with

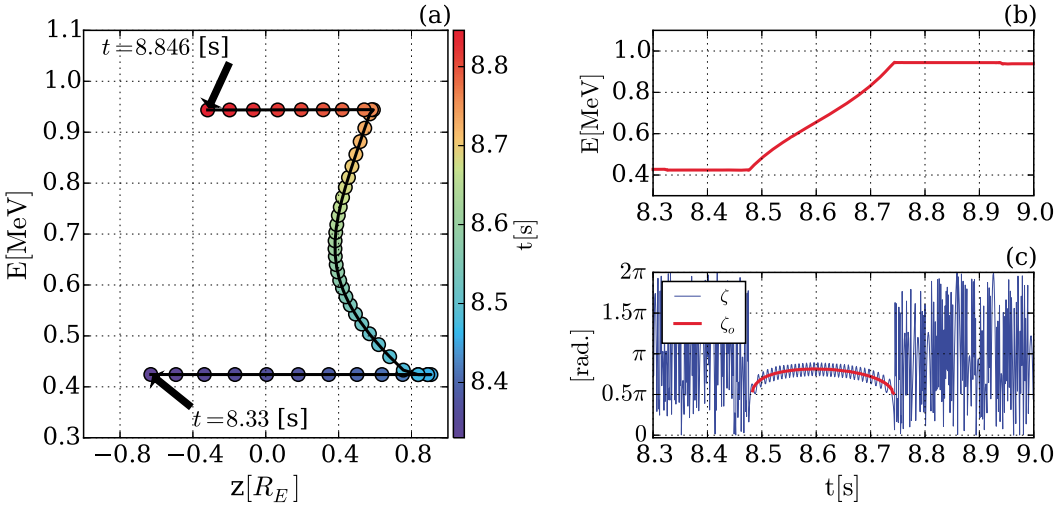

Figure 4. (a) Trajectory of the rapidly accelerated electron with $\alpha_{eq,init} = 60°$ from $t = 8.330$ to 8.846 s. (b) Time history of energy of the electron. (c) Blue line: The relative phase of the electron. (c) Red line: The stable equilibrium phase angle of the electron while it is phase trapped.

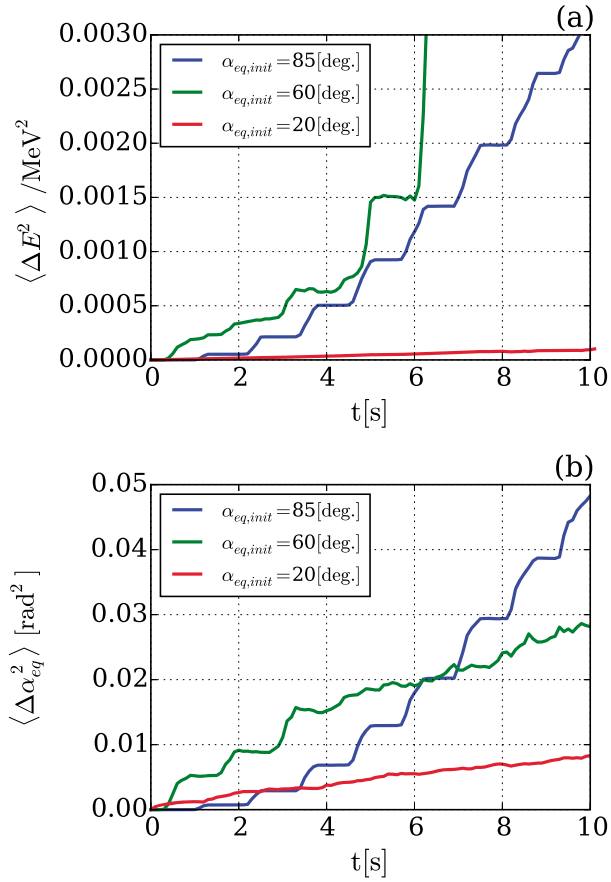

Figure 5. (a) Time history of the square of the energy change with three initial equatorial pitch angles. (b) Time history of the square of the equatorial pitch angle change with three initial equatorial pitch angles. These changes are averaged in 128 electrons in each run.

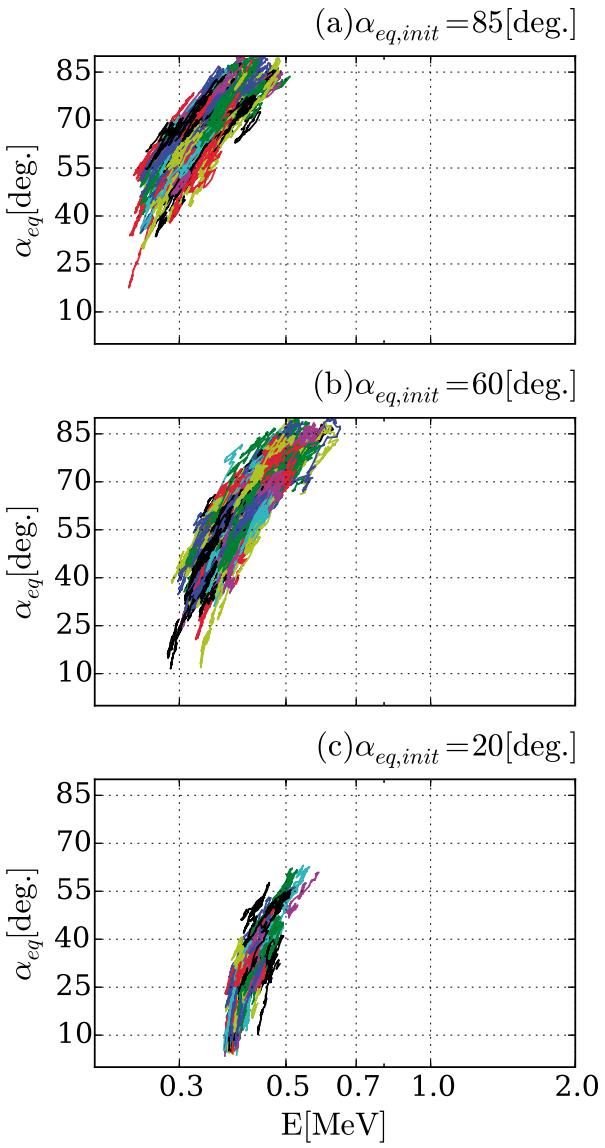

Figure 6. Same as Figure 1 but with the frequency of phase angle breaking 10^3 (Hz).

relativistic effect. Figure 4b shows the time history of energy of the electron. Figure 4c shows the relative phase angle ζ (blue line) that is $\phi_e - \phi_w$, where ϕ_e and ϕ_w are the electron gyrophase and the magnetic fluctuation phase. (For reference, see Figure 2 of *Omura et al.* [2007].) The red line of Figure 4c is the stable equilibrium angle ζ_o of the trapped electron, around which the electron revolves in the phase space (ζ, dζ/dt) as described in Appendix B. While increasing the energy as shown in Figure 4b, the phase angle ζ fluctuates coherently with a small variation around ζ_o. This indicates that the electron revolves around the equilibrium angle ζ_o in the phase space and is being phase trapped in the coherent whistler chorus element. All electrons accelerated to > 800 keV as shown in Figures 1 and 2 are phase trapped. The trapping is considered to occur probabilistically because the favorable resonance depends on latitude, pitch angle, and initial phase angle when the electron interacts with waves which satisfy the cyclotron resonance condition. Therefore, the nature of the scattering at this state is partially nonlinear and partially diffusive.

Figure 5 shows (a) the variation of energy $\langle \Delta E^2 \rangle$ and (b) the variation of equatorial pitch angle $\langle \Delta \alpha_{eq}^2 \rangle$, which are averaged by 128 electrons in each initial pitch angle ($\alpha_{eq,init}$ = 20°, 60°, and 85°). Here $\Delta E = E - 400$ keV and $\Delta \alpha_{eq} = \alpha_{eq} - \alpha_{eq,init}$. As the averaged quantities linearly increase in time, the scattering of electrons is in a quasi-linear diffusion process. As clearly seen in the panels, the scatterings with $\alpha_{eq,init}$ = 60° and 85° are

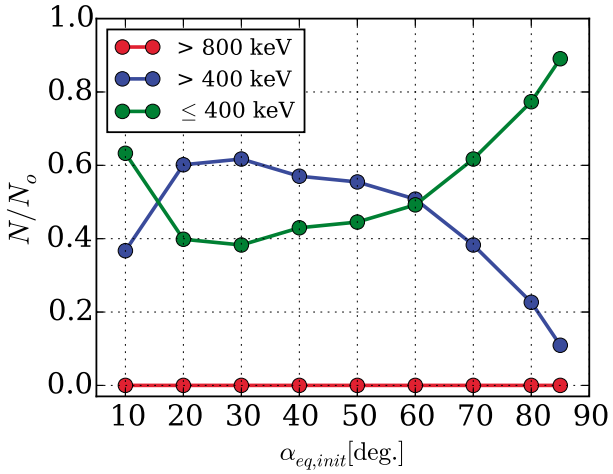

Figure 7. Same as Figure 2 but with the frequency of phase angle breaking 10^3 (Hz).

different from the quasi-linear diffusion process. Profiles of both $\langle \Delta E^2 \rangle$ and $\langle \Delta \alpha_{eq}^2 \rangle$ show step-like increases, indicating the nonlinear process. The step-like increase comes from the successive, discrete emissions of whistler chorus element. On the other hand, the electrons with $\alpha_{eq,init} = 20°$ increase almost linearly, suggesting that the scattering is close to the quasi-linear diffusion. This is consistent with the simulation result shown in Figures 1 and 2.

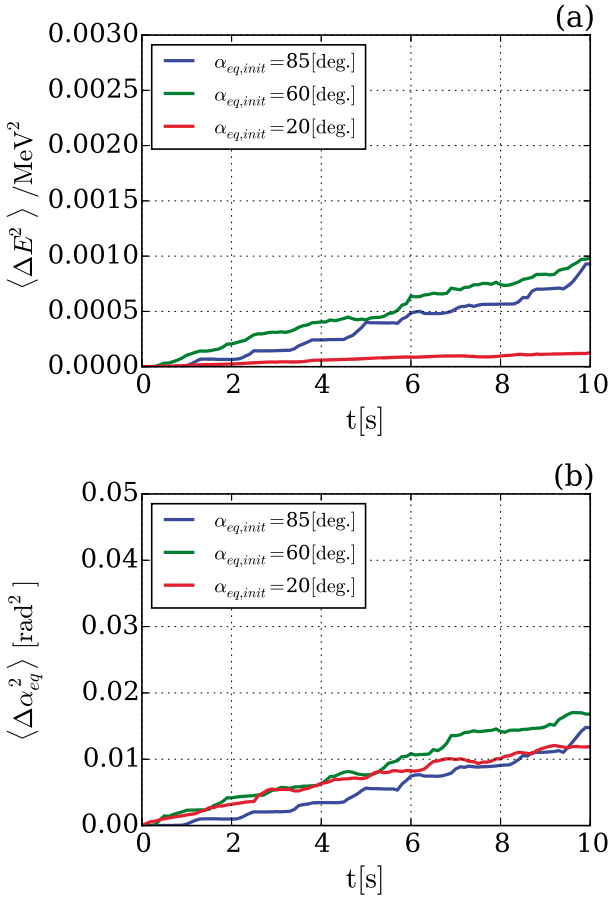

Figure 8. Same as Figure 5 but with the frequency of phase angle breaking 10^3 (Hz).

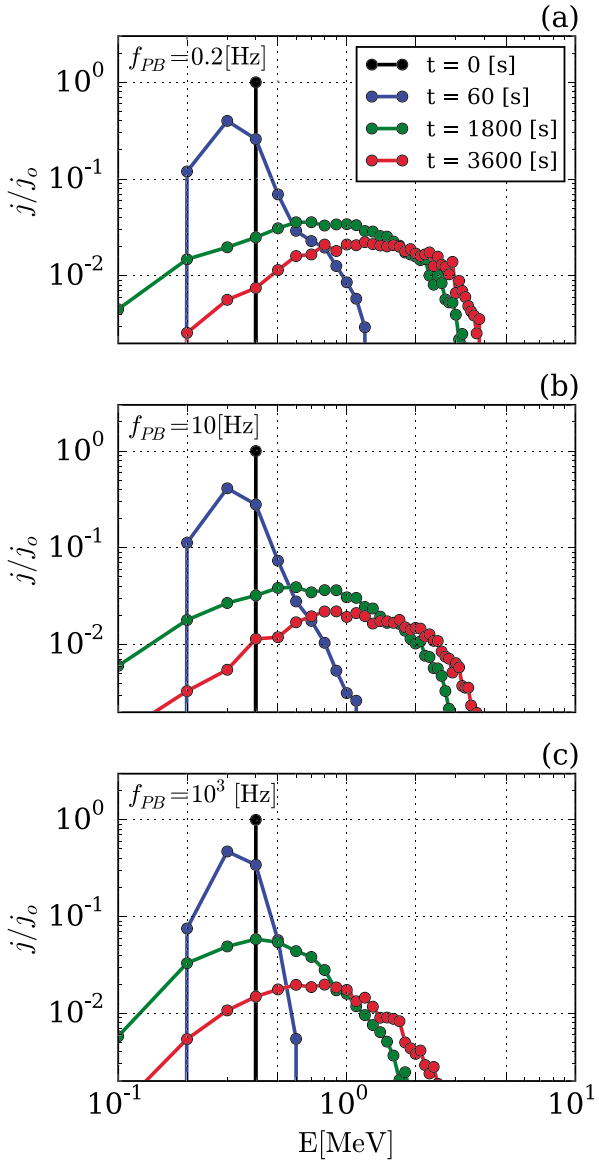

Figure 9. Time developments of the omnidirectional flux j as a function of energy, with (a) the frequency of the phase angle breaking 0.2 Hz, (b) 10 Hz, and (c) 1000 Hz. The flux is normalized by the initial omnidirectional flux j_o.

3.2. Electron Scattering by Whistler Chorus Elements With $f_{PB} = 10^3$ Hz

Figure 6 shows electron trajectories on (E, α_{eq}) plane during 60 s with $f_{PB} = 10^3$ Hz. The relative phase angle of electrons is forced to change every $f_{PB}^{-1} = 1$(ms) during the wave-particle interactions. Three panels have trajectories with initial equatorial pitch angle $\alpha_{eq,init}$ = (a) 85°, (b) 60°, and (c) 20°. Each simulation run has 128 electrons with kinetic energy of 400 keV at $t = 0$. As similar to simulation results with $f_{PB} = 0$ Hz (shown in Figure 1), kinetic energy of electrons increases (decreases) with increasing (decreasing) pitch angle. However, there is no remarkable acceleration of electrons to relativistic energies. The shapes of the trajectories in Figures 6a–6c are similar to each other. The behavior of the scattering seems to be diffusive.

Figure 7 is the same plot as Figure 2 but with $f_{PB} = 10^3$ Hz. Red, blue, and green lines show the number of remarkably accelerated electrons ($E \geq 800$ keV), accelerated electrons ($E > 400$ keV), and decelerated electrons ($E \leq 400$ keV) at 60 s, respectively. As clearly seen in the number of remarkably accelerated electrons (red line), there is no efficient acceleration of electrons with $f_{PB} = 10^3$ Hz. The phase trapping is forced to be suppressed by the frequent phase angle breaking. However, the initial pitch angle dependence of the

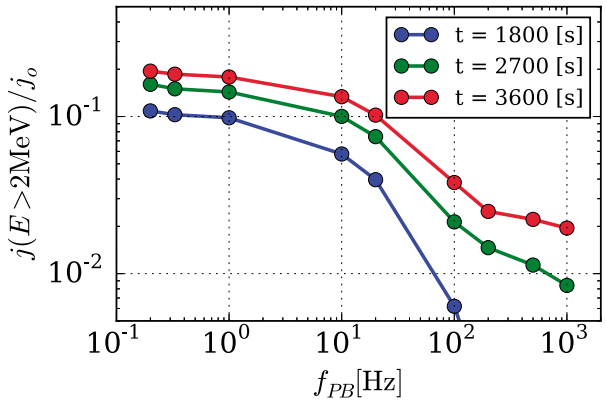

Figure 10. The flux integrated at larger than 2 MeV as a function of the frequency of the phase angle breaking.

number of accelerated (blue line) and decelerated (green line) electrons are similar to them without the phase angle breaking. The phase-bunching process at large pitch angle and diffusive process at small pitch angle are expected even with the high f_{PB}. It suggests that these scatterings are independent of the relative phase angle ζ. Only phase trapping is controlled by the phase angle breaking.

Figure 8 is the same plot as Figure 5 but with $f_{PB} = 10^3$ Hz. As expected from Figure 6, the time variation of the pitch angle and energy seems to be quasi-linear in these simulations, suggesting that the scattering process with $f_{PB} = 10^3$ Hz is similar to the quasi-linear diffusive in all pitch angles. However, in fact, the phase-bunching process is still effective as shown in Figure 7. The time variations of $\alpha_{eq,init} = 85°$ have the step-like feature similar to that shown in Figure 5, which comes from the collective deceleration of electrons by the successive and discrete emissions of whistler chorus elements.

3.3. Net Flux Enhancement as a Function of f_{PB}

We calculate temporal evolution of flux distribution of electrons which experience wave-particle interactions with whistler chorus elements propagating along the magnetic field line. The initial flux distribution is

$$j(E = 400\mathrm{keV}, \alpha_{eq}) = j_o \sin \alpha_{eq} \tag{1}$$

The number of test particles is 16,384 for each simulation run. Electrons with 400 keV are used as the initial condition. Figure 9 shows temporal evolution of omnidirectional differential flux at $t = 0$ (black), 60 (blue), 1800 (green), and 3600 s (red) as a function of energy. The frequency of the phase angle breaking is f_{PB} = (a) 0.2, (b) 10, and (c) 10^3 Hz. The flux is normalized to the initial omnidirectional flux. Rapid flux enhancement of MeV electrons in short time scale ($t = 60$ s), which is shown by the blue line of Figure 9a, is due to the phase trapping. We find that the flux enhancement is suppressed at higher f_{PB}, whose results can be expected from simulation results shown in sections 3.1 and 3.2. The flux enhancement is always faster than that with higher f_{PB}, indicating that the phase trapping is suppressed by the phase angle breaking. At $t = 60$ s, spectra at lower energies (< 400 keV) are quite similar to each other in three runs. At later times, however, flux of decelerated electrons becomes smaller at lower f_{PB}. This is because the phase-trapping process transports electrons from lower to higher energies.

Figure 10 shows the integral flux at > 2 MeV as a function of f_{PB}. Blue, green, and red lines are $t = 1800$, 2700, and 3600 s, respectively. The integral flux gradually increases in time, which is also shown in Figure 9. The flux enhancement is not a linear function of the frequency of the phase angle breaking. The flux distribution has spectral break frequencies at about $f_{PB} = 10$ Hz and 200 Hz. At the first breakpoint, the flux enhancement begins to be suppressed, while at the second breakpoint, the flux level becomes a rather weak function of f_{PB}. While the phase angle breaking does not strongly influences on the flux enhancement of relativistic electrons at lower f_{PB}, the flux enhancement is reduced as the phase angle breaking frequently occurs. When the frequency of the phase angle breaking is high enough, the phase angle breaking almost completely suppresses the phase trapping, so the flux increase is almost saturated at frequencies higher than the second breakpoint.

4. Discussion

Our simulation results for the coherent whistler chorus element ($f_{PB} = 0$ Hz) show three modes of scattering, which are diffusive, phase trapping, and phase bunching. Classification of the scattering processes can be described by the ratio of wave-induced and background inhomogeneity effects for the resonant electron [*Albert*, 2002; *Bortnik et al.*, 2008b]. According to *Inan et al.* [1978], the variation of the relative phase angle is given by a type of "pendulum" equation around the first-order resonant condition $v_\parallel \sim (\omega - \Omega_e)/k_\parallel$,

$$\frac{d^2\zeta}{dt^2} = k_\parallel v_\perp \Omega_w \sin\zeta + \left[\frac{3}{2} - \frac{\omega - \Omega_e}{2\Omega_e}\tan^2\alpha\right] v_\parallel \frac{\partial \Omega_e}{\partial z} \tag{2}$$

where ζ is the relative phase angle, ω is the angular frequency, $k_\parallel$ is the wave number parallel to the background magnetic field, $v_\parallel$ is the parallel velocity, $v_\perp$ is the perpendicular velocity, Ω_e is the electron angular cyclotron frequency, α is the pitch angle, and Ω_w is defined as eB_w/m_e, where e, m_e, and B_w are the absolute value of electron charge, the electron rest mass, and the magnetic wave amplitude, respectively. Note that we define the resonant electron velocity in the nonrelativistic regime as $v_\parallel \sim (\omega - \Omega_e)/k_\parallel$, while *Inan et al.* [1978] defined the velocity as $v_\parallel \sim (\Omega_e - \omega)/k_\parallel$ in equation (2). They defined a quantity which is the ratio of the coefficient of $\sin\zeta$ and the second term of the right-hand side of equation (2),

$$\rho = 2k_\parallel \Omega_w \tan\alpha \left[\left(3 - \frac{\omega - \Omega_e}{\Omega_e}\tan^2\alpha\right)\frac{\partial \Omega_e}{\partial z}\right]^{-1} \tag{3}$$

This quantity is the ratio of the wave-induced and the background inhomogeneity effects for the momentum change of the resonant electron. When the absolute value of the quantity is small enough ($|\rho| < 1$), the wave-induced effect for the resonant electron is less effective than the adiabatic effect related to the magnetic field inhomogeneity $\partial B_o/\partial z$. As described in *Bortnik et al.* [2008b], the wave-particle interaction with small $|\rho|$ causes a small, linear perturbation on the adiabatic momentum variation, indicating that the scattering by the wave shows the diffusive behavior. When the quantity is large enough ($|\rho| > 1$), the wave-induced effect is greater than the adiabatic effect. Then the nonlinear wave-particle interaction is expected. On the other hand, when the wave-induced and the adiabatic effects become comparable ($|\rho| \sim 1$), the coupling of two effects causes the remarkable nonlinear behavior—the nonlinear phase trapping. *Bortnik et al.* [2008b] proposed that three types of scattering behavior correspond to three types of interaction identified by *Albert* [2002], which are the diffusive ($|\rho| < 1$), the phase bunching ($|\rho| > 1$), and the phase trapping ($|\rho| \sim 1$). The ratio of the wave-induced and the background inhomogeneity effects can discriminate the nature of the scattering of electrons on the magnetic field line.

Equation (2) can be rewritten as

$$\frac{d^2\zeta}{dt^2} = k_\parallel v_\perp \Omega_w \left(\sin\zeta + \rho^{-1}\right) \tag{4}$$

This equation is similar to equation (10) of *Omura et al.* [2007] shown below,

$$\frac{d^2\zeta}{dt^2} = \frac{k_\parallel v_\perp \Omega_w \delta^2}{\gamma}(\sin\zeta + S) \tag{5}$$

where $\delta^2 = 1 - (\omega/ck_\parallel)^2$, γ is the relativistic Lorentz factor $[1 - (v_\parallel^2 + v_\perp^2)/c^2]^{-1/2}$, and S is the inhomogeneity ratio,

$$S = \frac{1}{2k_\parallel v_\perp \Omega_w \delta^2}\left[\left(2 + \delta^2\frac{\Omega_e - \gamma\omega}{\Omega_e - \omega}\right)V_R - \frac{k_\parallel \gamma v_\perp^2}{\Omega_e}\right]\frac{\partial \Omega_e}{\partial z} \tag{6}$$

where $V_R = (\omega - \Omega_e/\gamma)/k_\parallel$. Equation (5) describes the variation of the relative phase angle in almost the same theoretical model with *Inan et al.* [1978], but with the relativistic Lorentz factor γ. Comparing two equations, it is obvious that ρ^{-1} corresponds to the inhomogeneity ratio S. Thus, the absolute value of S^{-1} can be defined as the ratio of the wave-induced and the background inhomogeneity effects $\rho_\gamma = |S^{-1}|$ with the Lorentz factor. Three scattering modes, which are the diffusive, the phase trapping, and the phase bunching, can be classified by ρ_γ in the relativistic regime.

Figure 11 shows the equatorial pitch angle α_{eq} of electrons which satisfies the first-order resonance condition $\omega - k_\parallel v_\parallel - \Omega_e/\gamma = 0$ as a function of (a) latitude λ and (b) ρ_γ. Here we use same physical parameters shown in

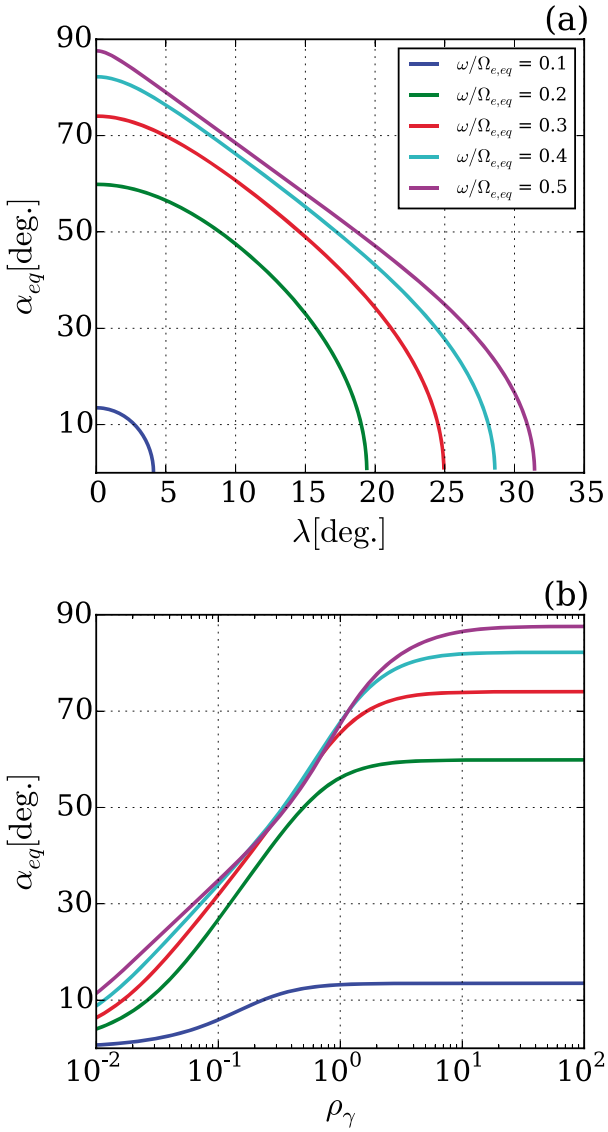

Figure 11. (a) Equatorial pitch angle of electron that resonates with whistler wave as a function of latitude. (b) Equatorial pitch angle of electron that resonates with whistler wave as a function of the ratio of wave-induced and background magnetic field inhomogeneity effects.

section 2. The resonant curves of Figure 11a shows that the equatorial pitch angle for each frequency becomes smaller at higher latitudes. Figure 11b shows that the electrons can resonate with whistler waves at smaller pitch angles with smaller ρ_γ. This suggests that the scattering is diffusive at smaller pitch angles, phase trapped at intermediate pitch angles, and collectively decelerated at large pitch angles.

The theoretical prediction is consistent with our simulation results. The numbers of decelerated and accelerated electrons are nearly equal at small pitch angles ($\alpha_{eq} < 50°$), and $\langle \Delta\alpha_{eq}^2 \rangle$ and $\langle \Delta E^2 \rangle$ with $\alpha_{eq} = 20°$ increase almost linearly (red lines in Figure 5). These results show that the scattering at small pitch angles can be considered as the diffusion process. Resonance for the electrons with smaller pitch angles occurs at higher latitudes where the background magnetic field inhomogeneity $\partial\Omega_e/\partial z$ becomes larger. Thus, ρ_γ tends to be small ($\rho_\gamma < 1$) at the small pitch angles. This result indicates that the scattering close to the loss cone angle, which causes the precipitation loss into the atmosphere, would be a dominantly diffusive process. However, discrete property of whistler chorus elements can lead to nondiffusive process of the precipitation [*Saito et al.*, 2012; *Miyoshi et al.*, 2015a, 2015b]. The nonlinearity originating from the discrete generation

process is also important to understand the physics associated with wave-particle interactions between whistler chorus waves and radiation belt electrons.

At intermediate pitch angles, which are around $\alpha_{eq} \sim 65°$ where $\rho_\gamma \sim 1$, the nonlinear phase trapping occurs efficiently (Figures 2 and 4). Further, at large pitch angles where $\rho_\gamma > 1$, our simulation confirms that the phase-bunching process becomes dominant (Figures 1–3). A few electrons are accelerated by the phase-trapping process even with $\alpha_{eq,init} = 85°$ as seen in Figures 1 and 3. These electrons are phase trapped after decreasing their pitch angle through the phase-bunching process.

The ratio of wave-induced and magnetic field inhomogeneity ρ_γ is a linear function of the wave amplitude. If the wave amplitude of whistler chorus element becomes over 1 nT which is 10 times larger than the amplitude used in our simulations, the equatorial pitch angle of phase-trapped electron becomes less than 30° as expected from Figure 11. Electrons at larger pitch angles ($\alpha_{eq} > 30°$) are scattered by the phase-bunching process leading collective deceleration. This fact suggests that larger-amplitude whistler waves decelerate electrons through the phase-bunching process more efficiently. Therefore, it may be considered that large-amplitude whistler waves contribute to reduce a net electron flux in the radiation belt through deceleration of electrons. Study for wave amplitude dependence of the net flux enhancement should be done as future works. Further, the resonance condition would change characteristics of wave-particle interactions, so dependence of background profiles (density and magnetic field strength along the field line) on the nonlinear interactions should be also focused as another work.

The scattering by whistler chorus waves along the field line tends to be diffusive at smaller pitch angles, phase trapped at intermediate pitch angles, and collectively decelerated at large pitch angles. Three scattering processes are classified by the ratio of wave-induced effect and background magnetic field inhomogeneity effect. In the dipole magnetic field, the magnetic field inhomogeneity becomes larger at higher latitudes. The equatorial pitch angle sets resonance point along the field line as shown in Figure 11a. Electrons with smaller pitch angles resonate with whistler wave at higher latitudes. It shows that smaller equatorial pitch angles lead to smaller ratio of wave-induced effect and background magnetic field inhomogeneity effect. Therefore, the scattering tends to be diffusive at smaller pitch angles (smaller ρ_γ), phase trapped at intermediate pitch angles (intermediate ρ_γ), and collectively decelerated at large pitch angles (larger ρ_γ). This trend is independent with energy.

The phase-trapping process is well affected by the phase angle breaking. By comparing between Figures 2 and 7, we find that large f_{PB} suppresses strong acceleration associated with the phase-trapping process (> 800 keV as shown by red line). On the other hand, diffusion and phase-bunching processes are not well affected by the phase angle breaking as shown by blue and green lines in Figures 2 and 7. In the definition of diffusion process, the wave-particle interaction does not depend on the relative phase. Further, as shown in *Bortnik et al.* [2008b], the phase-bunching process is independent of the relative phase. Thus, the scatterings by diffusion and phase-bunching processes are not well affected by the phase angle breaking during the wave-particle interaction. Figures 5 and 8 seem to show that the phase-bunching process is suppressed by the phase angle breaking, because electrons with $\alpha_{eq,init} = 85°$ are dominantly scattered by the phase-bunching process. Actually, some electrons with $\alpha_{eq,init} = 85°$ experience the strong acceleration by the phase-trapping process as shown in Figure 3a after the deceleration by the phase-bunching process. Only phase-trapping process, which is a source of efficient acceleration of electrons, is well suppressed by large f_{PB}.

We found two spectral breakpoints in the flux distribution shown in Figure 10. The first breakpoint appears around 10 Hz, and the other spectral breakpoint is about ~200 Hz. If the trapped electron is forced to leave from a closed trajectory of phase space (ζ, $d\zeta/dt$) to an opened trajectory through the phase angle breaking, then the phase trapping is stopped. The flux enhancement of relativistic electrons is expected to be suppressed if the time scale of f_{PB}^{-1} is less than the typical time scale of the phase trapping which accelerates electrons to relativistic energies. As shown in Figure 4, the trapping time for the efficient acceleration is of the order of 0.1 s which corresponds to 10 Hz. Thus, the first breakpoint is related to the time scale of phase trapping associated with the efficient acceleration. The second breakpoint could indicate the boundary where the nonlinear process competes with the quasi-linear process. Almost complete suppression of the phase trapping could lead to a stochastic process which is no longer dependent on the phase angle. The flux enhancement is almost flat at >200 Hz at $t = 3600$ s, so it is suggested that the scattering is almost stochastic at the frequency. As the phase trapping is suppressed at frequencies larger than the first breakpoint,

the flux enhancement becomes clearly slow. It can be concluded that the phase angle breaking has a remarkable role for the time scale of the flux enhancement of the relativistic electrons.

Recent observation [*Santolík et al.*, 2014] shows that a realistic whistler chorus element has fine structures consisting of a significant number of subpackets. Each subpacket has different properties (including wave amplitude and wave number vector) and so the phase-trapping condition could be dynamically changed. It is expected that the phase angle breaking frequently occurs in the whistler chorus element. Therefore, such a whistler chorus element may reduce the efficiency of flux enhancement of radiation belt electrons. The elementary nature of whistler chorus element should be studied and observed in more detail to understand net flux enhancement through wave-particle interactions.

In fact, whistler chorus waves are more oblique at higher latitudes, especially on the dayside [*Li et al.*, 2011]. The oblique whistlers lead to not only cyclotron resonance but also Landau resonance. We expect that the obliquity of whistlers at higher latitudes cannot substantially affect the nonlinear wave-particle interactions, because the momentum change associated with the wave-induced effect including Landau process is well smaller than the background inhomogeneity effect. Thus, the quasi-linear diffusion process could be dominant even with the obliquity at the high latitudes. On the other hand, if the obliquity is effective around the magnetic equator, Landau process might influence on nonlinear wave-particle interactions. The simulation for the oblique waves is out of the scope of the current GEMSIS-RBW simulation. The simulation study for the wave-particle interaction with the obliquity effect should be done by a newly developed model in the future.

Resonance condition depends on the magnetic field configurations and ambient plasma density distributions along the field lines. It is necessary to evaluate what condition lead to more/less efficient flux enhancement at MeV energy range, which should be subject for our future studies.

5. Summary

We investigated the net flux enhancement of relativistic electrons by wave-particle interactions with whistler chorus elements generated at the equator and focused on the origin of nonlinear scattering processes varying with the frequency of phase angle breaking in the chorus elements. The GEMSIS-RBW simulations confirmed three modes of scattering, which are diffusive, phase trapping, and phase bunching. While the diffusive process is relatively slow and quasi-linear process, the phase trapping and phase bunching are relatively fast and nonlinear process. In the three scattering modes, the phase-trapping process is the most efficient to accelerate electrons to relativistic energies. By comparing between the simulation with and without phase trapping, we conclude that the phase-trapping process has a remarkable role for the rapid flux enhancement at the relativistic energies.

It may be widely accepted that the long-term evolution of the distribution function after the multiple interactions with whistler chorus waves can be modeled as the diffusion process using the Fokker-Planck equation as the Markov process [e.g., *Walt*, 1994]. However, our simulation study shows that the phase-trapping process, which originates from the coherent whistler chorus elements, significantly contributes to the net flux enhancement of relativistic electrons even after multiple wave-particle interactions and even with diffusive and phase-bunching processes. It is implied that traditional diffusion theory with assumption of the Markov process does not always describe the net flux variations of the outer radiation belt properly. We expect that the contribution of the phase-trapping process, which is not described by the diffusion model, is essential for the rapid increase of the relativistic electron flux in the radiation belt.

Understanding the phase-trapping process is significant in order to clarify the acceleration of relativistic electrons in the magnetosphere. The acceleration of electrons by phase-trapping should be a universal process, not only in the terrestrial magnetosphere but also in the planetary magnetospheres [e.g., *Mauk and Fox*, 2010] and the solar atmosphere. The direct measurements of the phase trapping in the space plasma are currently being conducted by the newly developed wave-particle interaction analyzer on board the upcoming ERG satellite [*Miyoshi et al.*, 2012; *Katoh et al.*, 2013].

Appendix A: Basic Concept of GEMSIS-RBW Model

GEMSIS-RBW (Geospace Environment Modeling System for Integrated Studies-Radiation Belt with Wave-Particle Interaction) simulation code was developed to calculate nonlinear wave-particle interactions

between relativistic electrons and whistler chorus waves in the magnetosphere. This code calculates the guiding-center adiabatic motion of electrons trapped in a dipole magnetic field line, using the equations of motion for magnetic mirror force,

$$\frac{dp_{\parallel}}{dt} = -\frac{\mu}{\gamma}\frac{\partial B_o}{\partial z} \tag{A1}$$

$$\frac{dz}{dt} = v_{\parallel} \tag{A2}$$

where the first adiabatic invariant is $\mu = p_{\perp}^2/2m_eB_o$ and the relativistic factor is $\gamma = \left[1-(v_{\parallel}^2+v_{\perp}^2)/c^2\right]^{-1/2}$. Here B_o is the background magnetic field intensity, $p_{\parallel}$ is the momentum parallel to the background magnetic field, $p_{\perp}$ is the perpendicular momentum, $v_{\parallel}$ is the parallel velocity, $v_{\perp}$ is the perpendicular velocity, z is the position along the field line, m_e is the electron rest mass, and c is the speed of light. These equations are solved by fourth-order Runge-Kutta method with a time resolution Δt by considering that μ is conserved. The electron $p_{\perp}$ is updated by using μ at the electron position z. The equations numerically derive the adiabatic momentum change $\Delta\mathbf{p}_a$ for Δt.

The GEMSIS-RBW model calculates not only the adiabatic mirror motion but also the nonadiabatic momentum change by wave-particle interactions with whistler waves propagating along the magnetic field line. This model treats whistler chorus waves as wave packets. Each wave packet has a position z, an angular wave frequency ω, and amplitude of magnetic fluctuation B_w. The electric fluctuation amplitude is calculated as $E_w = (B_w\omega)/k_{\parallel}$, where the parallel wave number $k_{\parallel}$ is derived from a whistler dispersion relation in a cold plasma approximation. The magnetic fluctuation amplitude B_w and the frequency ω are constant, while the wave packet propagates to higher latitudes with its group velocity. Here the whistler dispersion relation used in this model is

$$k_{\parallel}^2 = \frac{\omega^2}{c^2}(1+\xi^{-2}) \tag{A3}$$

and the group velocity is

$$v_g = c\xi\sqrt{1+\xi^2}\left[\xi^2 + \frac{\Omega_e}{2(\Omega_e-\omega)}\right]^{-1} \tag{A4}$$

where

$$\xi^2 = \frac{\omega(\Omega_e-\omega)}{\omega_e^2} \tag{A5}$$

Ω_e is the electron cyclotron angular frequency, and ω_e is the electron plasma angular frequency. Ion contributions in the dispersion relation are ignored because the frequency range of whistler chorus wave is quite higher than that of the ion dynamics. Magnetic field intensity B and background electron density n_e are obtained at the wave packet position.

The RBW model generates a serial of whistler wave packets at the equator. The wave packets propagate parallel and antiparallel directions along the magnetic field line. Each electron on the field line can obtain wave information using a linear interpolation between nearest two packets.

As an electron is in a whistler chorus element, the equation of motion

$$\frac{d\mathbf{p}}{dt} = -e\left(\mathbf{E}_w + \mathbf{v}\times(\mathbf{B}_o+\mathbf{B}_w)\right) \tag{A6}$$

solves the electron momentum change of the electron, where e is the absolute value of electron charge, $\mathbf{p}$ is the electron momentum, $\mathbf{B}_o$ is the background magnetic field at the electron position, and $\mathbf{v}$ is the electron velocity. The Buneman-Boris method [*Buneman*, 1993] is used to solve the equation of motion with a time resolution Δt_w that is shorter enough than the electron cyclotron period at the position z. With the time resolution the equation of motion calculates the nonadiabatic momentum change $\Delta\mathbf{p}_w$ for Δt. Note that the background magnetic field $\mathbf{B}_o$ at the electron position is assumed to be constant during Δt ($\gg \Delta t_w$). Thus, the momentum change derived from equation (A6) is purely nonadiabatic. The nonadiabatic momentum change modifies the first adiabatic invariant by referring $\mathbf{B}_o$ at the electron position.

In order to solve the equation of motion in whistler wave, the relative phase angle between the electron and the wave should be considered properly. The time variation of electron gyration phase $d\phi_e/dt$ can be derived from equation (A6). The wave phase ϕ_w at the electron position is derived from

$$\frac{d\phi_w}{dt} = \omega - k_{\parallel} v_{\parallel} \tag{A7}$$

The time variation of the relative phase angle between the gyration phase and wave phase is calculated as

$$\frac{d\zeta}{dt} = \frac{d\phi_e}{dt} - \frac{d\phi_w}{dt} \tag{A8}$$

We consider intermittent wave phase angle breaking in a whistler chorus element and define that the relative phase angle ζ is updated with frequency f_{PB},

$$\zeta \leftarrow \delta_T R(\delta_T = 1) \tag{A9}$$

Here δ_T is a comb function with a period $T = f_{PB}^{-1}$, and R is a random function between 0 and 2π. The relative phase angle is randomly changed every T seconds that corresponds to a degree of incoherency in the whistler chorus element.

The GEMSIS-RBW model calculates both adiabatic momentum change $\Delta\mathbf{p}_a$ and nonadiabatic momentum change $\Delta\mathbf{p}_w$ during Δt. Thus, the full momentum change $\Delta\mathbf{p}$ for Δt is

$$\Delta\mathbf{p} = \Delta\mathbf{p}_a + \Delta\mathbf{p}_w \tag{A10}$$

The coupled momentum change $\Delta\mathbf{p}$ updates the electron momentum $\mathbf{p} + \Delta\mathbf{p} \rightarrow \mathbf{p}$ at the next time step $t + \Delta t \rightarrow t$.

The RBW model ignores any feedbacks from relativistic electrons to the electromagnetic fields. This approximation is always valid in the radiation belt because the high-energy electrons (greater than a few hundred keV) are tenuous compared with background electron population that is a free energy source for whistler mode waves.

Appendix B: Equilibrium Phase Angle of Trapped Electron

As derived in *Omura et al.* [2007], the second-order nonlinear ordinary differential equation for the relative phase angle is

$$\frac{d\zeta^2}{dt^2} = \frac{\omega_t^2 \delta^2}{\gamma} (\sin\zeta + S) \tag{B1}$$

where $\delta^2 = 1 - \omega^2/c^2k_{\parallel}^2$, $\omega_t^2 = k_{\parallel} v_{\perp} \Omega_w$, $v_{\perp} = p_{\perp}/m_e\gamma$, and $\Omega_w = eB_w/m_e$. The parameter S is the inhomogeneity ratio [e.g., *Omura et al.*, 2007, 2009]. Figure B1 shows trajectories of electrons interacting with whistler

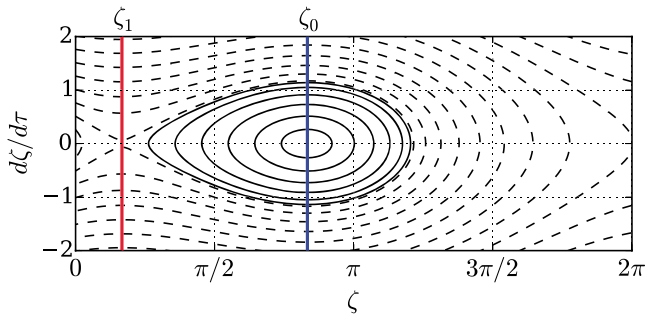

Figure B1. Trajectories of electrons interacting with whistler chorus wave in the phase space of the relative phase angle for the inhomogeneity ratio $S = -0.5$. Solid and dashed black lines are closed and opened trajectories, respectively. The red and blue lines are an unstable saddle and stable equilibrium angle, where the first-order resonance condition is satisfied.

chorus wave in the phase space $(\zeta, d\zeta/d\tau)$ for the inhomogeneity ratio $S = -0.5$, where $\tau^2 = \omega_t^2\delta^2\gamma^{-1}t$. Solid and dashed black lines are closed and opened trajectories, respectively. Red and blue lines show phase angles ζ_0 and ζ_1 when $d\zeta^2/d\tau^2 = 0$,

$$\sin\zeta + S = 0 \tag{B2}$$

Two solutions exist when $|S| < 1$, which are $\zeta_1 = \sin^{-1}(-S)$ and $\zeta_0 = \pi - \zeta_1$. If $S = -0.5$ as used in Figure B1, then $\zeta_0 = 5\pi/6$ and $\zeta_1 = \pi/6$. The phase angles ζ_0 and ζ_1 represent a stable equilibrium point and a unstable saddle point on $d\zeta/d\tau = 0$ line, respectively. The phase-trapped electron revolves around the stable point in time. Since the inhomogeneity ratio determines the equilibrium point ζ_0 and the saddle point ζ_1, the inhomogeneity ratio is the key parameter for the phase-trapping region in the phase space. When the trajectory of the trapped electron has $\zeta < \pi$, the electron can stably gain energy from the electric fluctuation of the whistler wave. Note that the phase angle of the electric fluctuation is 90° behind of the magnetic fluctuation. Actually, the inhomogeneity ratio is variable in time and space. If the trapped electron moves to place where $|S| > 1$ during the wave-particle interaction, the electron is released from the phase-trapping region and stops the stable energy gain from the whistler wave. Further, if the phase angle breaking transports the electron from closed to opened trajectory in the phase space $(\zeta, d\zeta/d\tau)$, then the electron also stops the energy gain.

Acknowledgments
This work is supported by JSPS KAKENHI grants 23340146, 15H05747 and 15H05815 and the GEMSIS project at ISEE/Nagoya University. This work is also supported by JSPS Program for Advancing Strategic International Networks to Accelerate the Circulation of Talented Researchers under grant G2602. The simulation data presented in this paper can be obtained by contacting the first author S.S.

References

Albert, J. M. (2002), Nonlinear interaction of outer zone electrons with VLF waves, *Geophys. Res. Lett.*, *29*(8), 1275, doi:10.1029/2001GL013941.

Bortnik, J., R. M. Thorne, and N. P. Meredith (2008a), The unexpected origin of plasmaspheric hiss from discrete chorus emissions, *Nature*, *452*, 62–66, doi:10.1038/nature06741.

Bortnik, J., R. M. Thorne, and U. S. Inan (2008b), Nonlinear interaction of energetic electrons with large amplitude chorus, *Geophys. Res. Lett.*, *35*, L21102, doi:10.1029/2008GL035500.

Bortnik, J., W. Li, R. M. Thorne, V. Angelopoulos, C. Cully, J. Bonnell, O. Le Contel, and A. Roux (2009), An observation linking the origin of plasmaspheric hiss to discrete chorus emissions, *Science*, *324*(5928), 775–778, doi:10.1126/science.1171273.

Buneman, O. (1993), TRISTAN, in *Computer Space Plasma Physics: Simulation Techniques and Software*, edited by H. Matsumoto and Y. Omura, pp. 67–84, Terra Sci., Tokyo.

Chen, Y., G. D. Reeves, and R. H. W. Friedel (2007), The energization of relativistic electrons in the outer Van Allen radiation belt, *Nat. Phys.*, *3*, 614–617, doi:10.1038/nphys655.

Elkington, S. R., M. K. Hudson, and A. A. Chan (1999), Acceleration of relativistic electrons via drift-resonant interaction with toroidal-mode Pc-5 ULF oscillations, *Geophys. Res. Lett.*, *26*(21), 3273–3276, doi:10.1029/1999GL003659.

Furuya, N., Y. Omura, and D. Summers (2008), Relativistic turning acceleration of radiation belt electrons by whistler mode chorus, *J. Geophys. Res.*, *113*, A04224, doi:10.1029/2007JA012478.

Horne, R. B., R. M. Thorne, S. A. Glauert, J. M. Albert, N. P. Meredith, and R. R. Anderson (2005), Timescale for radiation belt electron acceleration by whistler mode chorus waves, *J. Geophys. Res.*, *110*, A03225, doi:10.1029/2004JA010811.

Inan, U. S., T. F. Bell, and R. A. Helliwell (1978), Nonlinear pitch angle scattering of energetic electrons by coherent VLF waves in the magnetosphere, *J. Geophys. Res.*, *83*(A7), 3235–3253, doi:10.1029/JA083iA07p03235.

Katoh, Y., et al. (2013), Significance of wave-particle interaction analyzer for direct measurements of nonlinear wave-particle interactions, *Ann. Geophys.*, *31*, 503–512, doi:10.5194/angeo-31-503-2013.

Li, W., J. Bortnik, R. M. Thorne, and V. Angelopoulos (2011), Global distribution of wave amplitudes and wave normal angles of chorus waves using THEMIS wave observations, *J. Geophys. Res.*, *116*, A12205, doi:10.1029/2011JA017035.

Mauk, B. H., and N. J. Fox (2010), Electron radiation belts of the solar system, *J. Geophys. Res.*, *115*, A12220, doi:10.1029/2010JA015660.

Macúšová, E., O. Santolik, N. Cornilleau-Wehrlin, and K. H. Yearby (2015), Bandwidths and amplitudes of chorus-like banded emissions measured by the TC-1 Double Star spacecraft, *J. Geophys. Res. Space Physics*, *120*, 1057–1071, doi:10.1002/2014JA020440.

Meredith, N. P., R. B. Horne, D. Summers, R. M. Thorne, R. H. A. Iles, D. Heynderickx, and R. R. Anderson (2002), Evidence for acceleration of outer zone electrons to relativistic energies by whistler mode chorus, *Ann. Geophys.*, *20*, 967–979, doi:10.5194/angeo-20-967-2002.

Miyoshi, Y., A. Morioka, T. Obara, H. Misawa, T. Nagai, and Y. Kasahara (2003), Rebuilding process of the outer radiation belt during the 3 November 1993 magnetic storm: NOAA and Exos-D observations, *J. Geophys. Res.*, *108*(A1), 1004, doi:10.1029/2001JA007542.

Miyoshi, Y., A. Morioka, R. Kataoka, Y. Kasahara, and T. Mukai (2007), Evolution of the outer radiation belt during the November 1993 storms driven by corotating interaction regions, *J. Geophys. Res.*, *112*, A05210, doi:10.1029/2006JA012148.

Miyoshi, Y., et al. (2012), The Energization and Radiation in Geospace (ERG) project, in *Dynamics of the Earth's Radiation Belts and Inner Magnetosphere*, edited by D. Summers et al., pp. 103–116, AGU, Washington, D. C., doi:10.1029/2012GM001304.

Miyoshi, Y., R. Kataoka, Y. Kasahara, A. Kumamoto, T. Nagai, and M. F. Thomsen (2013), High-speed solar wind with southward interplanetary magnetic field causes relativistic electron flux enhancement of the outer radiation belt via enhanced condition of whistler waves, *Geophys. Res. Lett.*, *40*, 4520–4525, doi:10.1002/grl.50916.

Miyoshi, Y., et al. (2015a), Energetic electron precipitation associated with pulsating aurora: EISCAT and Van Allen Probe observations, *J. Geophys. Res. Space Physics*, *120*, 2754–2766, doi:10.1002/2014JA020690.

Miyoshi, Y., et al. (2015b), Relation between fine structure of energy spectra for pulsating aurora electrons and frequency spectra of whistler mode chorus waves, *J. Geophys. Res. Space Physics*, *120*, 7728–7736, doi:10.1002/2015JA021562.

Omura, Y., N. Furuya, and D. Summers (2007), Relativistic turning acceleration of resonant electrons by coherent whistler mode waves in a dipole magnetic field, *J. Geophys. Res.*, *112*, A06236, doi:10.1029/2006JA012243.

Omura, Y., M. Hikishima, Y. Katoh, D. Summers, and S. Yagitani (2009), Nonlinear mechanisms of lower-band and upper-band VLF chorus emissions in the magnetosphere, *J. Geophys. Res.*, *114*, A07217, doi:10.1029/2009JA014206.

Reeves, G. D., et al. (2013), Electron acceleration in the heart of the Van Allen radiation belts, *Science*, *341*, 991–994, doi:10.1126/science.1237743.

Saito, S., Y. Miyoshi, and K. Seki (2012), Relativistic electron microbursts associated with whistler chorus rising tone elements: GEMSIS-RBW simulations, *J. Geophys. Res.*, *117*, A10206, doi:10.1029/2012JA018020.

Santolík, O., D. A. Gurnett, J. S. Pickett, M. Parrot, and N. Cornilleau-Wehrlin (2003), Spatio-temporal structure of storm-time chorus, *J. Geophys. Res.*, *108*(A7), 1278, doi:10.1029/2002JA009791.

Santolík, O., C. A. Kletzing, W. S. Kurth, G. B. Hospodarsky, and S. R. Bounds (2014), Fine structure of large-amplitude chorus wave packets, *Geophys. Res. Lett.*, *41*, 293–299, doi:10.1002/2013GL058889.

Summers, D., R. M. Thorne, and F. Xiao (1998), Relativistic theory of wave-particle resonant diffusion with application to electron acceleration in the magnetosphere, *J. Geophys. Res.*, *103*(A9), 20,487–20,500, doi:10.1029/98JA01740.

Summers, D., Y. Omura, S. Nakamura, and C. A. Kletzing (2014), Fine structure of plasmaspheric hiss, *J. Geophys. Res. Space Physics*, *119*, 9134–9149, doi:10.1002/2014JA020437.

Thorne, R. M., E. J. Smith, R. K. Burton, and R. E. Holzer (1973), Plasmaspheric hiss, *J. Geophys. Res.*, *78*(10), 1581–1596, doi:10.1029/JA078i010p01581.

Thorne, R. M., et al. (2013), Rapid local acceleration of relativistic radiation-belt electrons by magnetospheric chorus, *Nature*, *504*, 411–414, doi:10.1038/nature12889.

Walt, M. (1994), *Introduction to Geomagnetically Trapped Radiation*, Cambridge Univ. Press, Cambridge, U. K.